

Article

Estimation of Indoor ^{222}Rn Concentration in Lima, Peru Using LR-115 Nuclear Track Detectors Exposed in Different Modes

Patrizia Pereyra ^{1,*} , Cesar J. Guevara-Pillaca ^{1,2}, Rafael Liza ^{1,3} , Bertin Pérez ^{1,4,5} , Jhonny Rojas ¹ , Luis Vilcapoma L. ¹, Susana Gonzales ⁶, Laszlo Sajo-Bohus ^{7,8}, María Elena López-Herrera ¹ and Daniel Palacios Fernández ¹

¹ Departamento de Ciencias, Pontificia Universidad Católica del Perú, Lima 15088, Peru; cesarj.guevara@pucp.edu.pe (C.J.G.-P.); raliza@pucp.edu.pe (R.L.); bertin.perez@pucp.edu.pe (B.P.); jrojash@pucp.edu.pe (J.R.); lvilcapoma@pucp.edu.pe (L.V.L.); mlopez@pucp.edu.pe (M.E.L.-H.); dpalaciosf@pucp.edu.pe (D.P.F.)

² Instituto Geológico, Minero y Metalúrgico INGEMMET, Lima 15034, Peru

³ Facultad de Ingeniería, Universidad Tecnológica del Perú, Lima 15046, Peru

⁴ Rad Elec Inc., Frederick, MD 21704, USA

⁵ Investigación, Desarrollo e Innovación, Anphysrad SAC, Lima 15074, Peru

⁶ Instituto Peruano de Energía Nuclear IPEN, Lima 15034, Peru; sgonzales@ipen.gob.pe

⁷ Nuclear Laboratory, Universidad Simón Bolívar, Caracas 1080 A, Venezuela; lsajo@usb.ve

⁸ Alba Regia Technical Faculty, Óbuda University, 800 Szekesfehervar, Hungary

* Correspondence: ppereyr@pucp.edu.pe

Abstract: Radon is the main source of natural radioactivity, and its measurement is considered extremely important in radioprotection, given its relationship with the occurrence of lung cancer. In the last two years, measurements of this radioactive gas were carried out in Lima considering a grid of 5 km² and the population density to determine the number of measurements to be carried out. Cellulose nitrate nuclear track detectors exposed in bare mode and diffusion chamber mode were used to estimate ^{222}Rn concentrations. In diffusion chamber mode, non-commercial monitors and commercial monitors were used. The monitoring results are presented for 43 districts of the Lima Province whose population is approximately ten million inhabitants occupying a total area of 2655.15 km². Measurements were made obtaining an average concentration of 49 Bq·m⁻³ using bare detectors and 66 Bq·m⁻³ using non-commercial diffusion chambers. Average concentrations obtained by both detector exposure modes were below the maximum concentration recommended by the WHO. A radon (^{222}Rn) map was also obtained as a visual representation of the ^{222}Rn levels in the Lima province using inverse distance weighting (IDW) interpolation.

Keywords: ^{222}Rn ; nuclear track detectors; cellulose nitrate; monitoring



Citation: Pereyra, P.; Guevara-Pillaca, C.J.; Liza, R.; Pérez, B.; Rojas, J.; Vilcapoma L., L.; Gonzales, S.; Sajo-Bohus, L.; López Herrera, M.E.; Palacios Fernández, D. Estimation of Indoor ^{222}Rn Concentration in Lima, Peru Using LR-115 Nuclear Track Detectors Exposed in Different Modes. *Atmosphere* **2023**, *14*, 952. <https://doi.org/10.3390/atmos14060952>

Academic Editors: Qiuju Guo and Mirosław Janik

Received: 18 April 2023

Revised: 15 May 2023

Accepted: 24 May 2023

Published: 30 May 2023



Copyright: © 2023 by the authors. Licensee MDPI, Basel, Switzerland. This article is an open access article distributed under the terms and conditions of the Creative Commons Attribution (CC BY) license (<https://creativecommons.org/licenses/by/4.0/>).

1. Introduction

Human beings are continuously exposed to ionizing radiation. The majority of the population considers that this has its origin only artificially, when in reality, the greatest contribution comes from nature. Human beings receive radioactive natural doses mainly through (i) gamma radiation, (ii) ^{222}Rn and ^{220}Rn with their progenies (present in the air), and (iii) radioisotopes present in water and food. Of these three sources, radon isotopes (^{222}Rn and ^{220}Rn , with the latter having sometimes having been historically named ‘thoron’) together with their short-lived progeny, mostly alpha emitters, account for just over 50% of the natural radiation contribution received by a human being [1]. Radon gas has a naturally occurring radioisotope ^{222}Rn from the ^{238}U chain, which has a half-life of 3.825 days and emits alpha particles of 5.48 MeV; its predecessor is ^{226}Ra . ^{222}Rn is present in the air and its progeny (^{218}Po , ^{214}Po), which are short-lived alpha emitters, adhere to environmental dust particles to form aerosols that enter into the human respiratory tract. When these aerosols are inhaled and attached in the tracts, they can cause damage to the lungs and

respiratory tract by altering DNA strands. Various epidemiological studies indicate the relationship between radon and the incidence of lung cancer [2–6]. It has been reported that the risk of lung cancer increases linearly with the concentration of radon and that there is no threshold beyond which the effect is harmless [7]. Initially, the risk of lung cancer was associated exclusively with the high risk that miners are exposed to, but in 1984, a house was incidentally found with ^{222}Rn levels close to $100,000 \text{ Bq}\cdot\text{m}^{-3}$, which is comparable to the previous case [8]. From that moment on, ^{222}Rn measurements inside homes took importance [9]; several works have reported measurements, monitoring, and ^{222}Rn maps of countries and continents using different methodologies and scopes [10–15]. Radon in houses comes not only from the subsoil, but also from construction materials, coatings, pipes, and domestic water, and its concentration is affected by atmospheric and ventilation factors.

Monitoring systems have been used to evaluate the indoor radon concentration and, in some cases, relate its presence to the risk of developing neoplasia [16]. Additionally, they are used for several purposes, such as to identify radon priority areas, for identifying areas to prioritize mitigation, for developing policies, and for programs to reduce indoor radon air levels. These applications may include measures such as promoting the construction of low-radon-emitting homes and implementing building codes, which can also help to understand the relationship between the distribution of radon gas and its relationship with other environmental and geogenic factors.

Long-term and large-scale measurements with solid-state nuclear track detectors (SSNTDs) have been carried out in many countries to identify dwellings with high ^{222}Rn levels [17–19]. Currently, CR-39 (poly allyl glycol carbonate) detectors are the most widely used SSNTDs for indoor ^{222}Rn measurements [20–24]. However, in this work, we chose the non-strippable LR-115 type 2 detector due to its low cost and its suitability for use in both bare mode [25–27] and inside a diffusion chamber [28,29].

The LR-115 detector exposed in bare mode registers alpha tracks from airborne concentrations of ^{222}Rn and ^{220}Rn and their alpha emitting progeny, but they do not detect the alpha activity deposited on the detector [30]. This mode of exposure leads to large uncertainties in the estimation of the ^{222}Rn concentration, since the same ^{222}Rn concentration value can be associated with different concentrations of its progeny depending on various atmospheric factors [31]. This is also further complicated if ^{220}Rn and its non-equilibrated progeny are present. That is why its calibration in the laboratory may not be adequate for indoor conditions. The determination of ^{222}Rn concentrations strongly depends on equilibrium factor, which is estimated between 0.2 and 0.7 for typical indoor conditions [1]. Thus, the value of the equilibrium factor must be within this range when calibrating bare detectors.

The estimation of ^{222}Rn concentrations using diffusion chambers is direct and univocal, and its calibration is easier than bare detectors, because only ^{222}Rn is registered. These monitors are less sensitive to environmental conditions [32], and exposure time could be larger than in the case of bare detectors. Among the disadvantages, we can mention its higher cost and its higher probability of getting lost compared to bare detectors mounted on the wall. Generally, diffusion chambers limit the ingress to its internal volume for aerosols and progeny water vapor, thereby discriminating ^{222}Rn from ^{220}Rn .

The objective of this work was to determine the indoor ^{222}Rn concentrations in Lima, Peru using non-strippable LR-115 type 2 detectors exposed in bare mode and inside diffusion chambers. Results for each mode were compared between each other and with the reference level recommended by the WHO and IPEN [29,33].

To meet this objective, a survey was carried out, where the LR-115 detector exposed in bare mode was used as a ^{222}Rn monitor. To complement the previous statement, two types of ^{222}Rn monitors based on LR-115 detectors and diffusion chambers were also used: one commercial and the other homemade. The ^{222}Rn map was also obtained as a visual representation of ^{222}Rn levels in the Lima province.

2. Materials and Methods

2.1. Description of Study Location

Lima, capital of Peru, is located on the central and western coast of South America. Its location is on a desert strip that extends from north to south between the Pacific Ocean and the Andean mountain range. The city mostly lies on flat terrain within the valleys of the Chillón, Rimac, and Lurín rivers, which drain into the Pacific Ocean. The Chillón River is located to the north of Lima, the Rimac River in the center, and the Lurín River to the south of the capital city. These rivers have played a vital role in the erosion and transportation of unconsolidated materials caused by the denudation of hills along their courses. The geology of the studied area has been described in a previous work [34]. The study area, also known as Metropolitan Lima, is divided into districts, which were grouped into 4 zones for this study: Lima Centro, Lima Este, Lima Norte, and Lima Sur [35].

Lima Centro is located in the metropolitan area center and comprises sixteen districts with an area of 147.73 km² and a population of 2,155,132 inhabitants [36]; it is the area with the highest population density of Lima. The soils in this zone have been formed mainly by alluvial deposits brought by the Rimac River. In addition, the water table is predominantly deep, and there are organic deposits that increase soil compaction in this area. There are some rocky outcrops in the zone that have been covered by silty and clayey materials. The conglomerate in this zone contains gravelly material that varies in density from loose to compact. This material is also mixed with layers of medium to fine sand, silt, and clay with a small amount of fine particles [37].

Lima Este is located in the eastern part of the metropolitan area and comprises eight districts with an area of 814.25 km² and a population of 2,937,764 inhabitants. In this zone, there are colluvial deposits due to the effect of gravity (e.g., San Juan de Lurigancho). The displacement of this eroded material has been very slow, but due to urban growth, there is the additional presence of fill material deposits formed by borrowed material, wastes, and debris that come from other zones [37]. The soil in this zone also presents alluvial deposits characterized by the presence of rounded cobblestone material.

Lima Norte is located in the northern part of the metropolitan area and comprises eight districts with an area of 857.26 km² and a population of 2,917,414 inhabitants. Colluvial and alluvial deposits over this zone have been covered over time by shallow stratas of fine granular and clayey materials [37]. These materials traveled across the Chillón River, starting their erosive detachment from the Nevado de la Viuda and surrounding areas.

Lima Sur is located in the southern part of the metropolitan area and comprises eleven districts with an area of 845.92 km² and a population of 2,901,224 inhabitants. This zone has eolian deposits [38] caused by strong winds from the south, and it is predominantly dry. Lima Sur also has marine deposits associated with its topography. These types of deposits increase the level of soil porosity, which can have an impact on indoor ²²²Rn concentration.

Districts with low population densities have not been considered a priority in the surveys. The study area covers a total surface of 2819.26 km², with a currently estimated population of 10,178,810 inhabitants [39].

Lima is one of the few capitals in the world located on the coast of a desert area. The monitoring area is shown in Figure 1. The climate in Lima is classified as hot arid (BWh) according to the Köppen–Geiger classification [40]. Lima is characterized by very low rainfall (annual average 7 mm); however, its relative humidity is quite high (reaching 99% in winter), and there is persistent cloudiness. Typically, temperatures range from 12 to 30 °C [41].

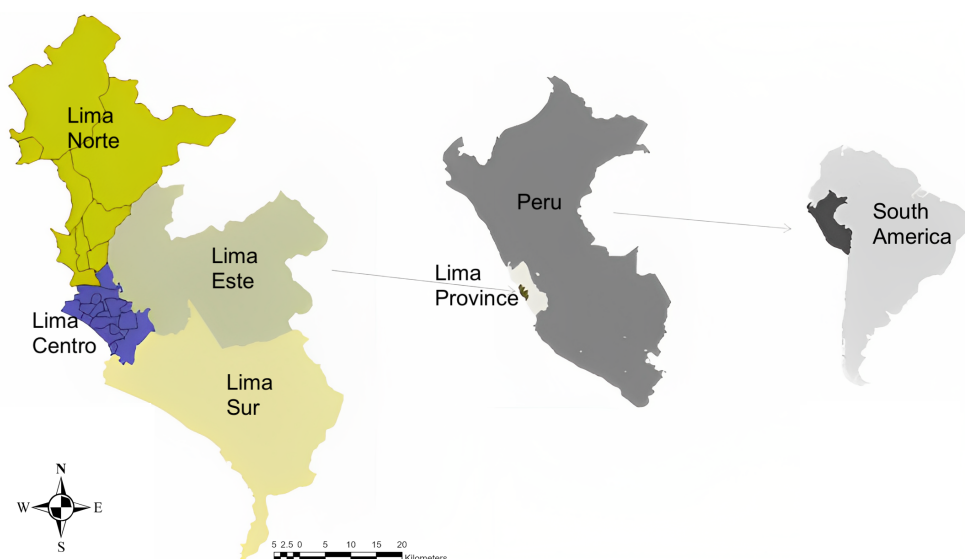


Figure 1. Map of the studied areas in Lima province. The scale only refers to the left map.

2.2. Site-Selection Criteria

A similar site-selection criterion to those carried out in other countries [42–45] was adopted. In order to ensure that the sampling accurately represented the entire population under investigation, stratified sampling was employed through the use of grids, wherein a random sampling was conducted within each grid. As per [44] findings, this methodology is an effective means of ensuring sample representativeness. The criterion consisted of sectioning each district in a grid system of 5 km², where a minimum number of dwellings or working places per grid was chosen according to Table 1.

Table 1. Criteria to determine the minimum number of sampled dwellings per grid.

District Type	Population Density (inhabitants·km ⁻²)	Number of Sampled Dwellings by Grid (Minimum)
A	≤2500	none
B	≤5000	1
C	≤10,000	2
D	≤20,000	4
E	≥20,000	6

Since the study was carried out for research purposes by our research group (GITHUNU—PUCP [Available online: <https://investigacion.pucp.edu.pe/grupos/githunu/> (accessed on 7 May 2023)]), sampling dwellings were member’s homes of our community university, who voluntarily carried some monitors to their homes after internal awareness campaigns (e.g., website, videos, digital media) in order to motivate participation. They filled out a google form with information about monitoring places (Appendix A).

It is worth mentioning that this monitoring was the first of its kind conducted in our country on a medium regional scale. Since the focus of measurements was to determine the ²²²Rn concentration indoors, a minimum number of detectors was established per district based on the population density in each district [29]. This criterion was assumed based on available resources for ²²²Rn concentration measurements. Although no sampling dwellings were planned for type A districts, some measurements were made thanks to the participation of volunteers.

To calculate the minimum number of dwellings to sample in each district, the habitable area of each district was divided by the grid area. The data presented in Table 2 corresponds to the estimated population.

Table 2. Number of ²²²Rn monitors and dwellings sampled by grid cells in each district based on the estimated population.

Zones	District	Population Density * (inhabitants·km ⁻²)	Sampled Dwellings per Grid (Minimum)	Number of Grids (Urban Zone)	Number of Monitors (Minimum)	Number of Monitors (Real)
Lima Centro	Barranco	10,951	2	1	2	3
	Breña	29,561	6	1	6	16
	Cercado de Lima	12,198	4	4	16	31
	Jesús María	18,360	4	1	4	13
	La Victoria	21,693	6	2	12	9
	Lince	20,359	4	1	4	7
	Magdalena del Mar	18,770	4	1	4	7
	Miraflores	11,799	4	2	8	10
	Pueblo Libre	22,276	6	1	6	50
	Rímac	15,407	4	2	8	5
	San Borja	13,141	4	2	8	11
	San Isidro	6253	2	2	4	10
	San Luis	16,132	4	1	4	12
	San Miguel	16,851	4	2	8	35
Surco	12,087	4	7	28	22	
Surquillo	29,605	6	1	6	6	
Lima Este	Ate	9043	2	7	14	26
	Cieneguilla	167	0	1	0	0
	Chaclacayo	1142	0	1	0	2
	El Agustino	18,296	4	1	4	1
	La Molina	2510	1	5	5	11
	Lurigancho	1279	0	1	0	0
	San Juan de Lurigancho	9334	2	18	36	29
Santa Antita	21,284	6	12	72	7	
Lima Norte	Ancon	306	0	1	0	0
	Carabayllo	1222	0	1	0	0
	Comas	12,039	4	10	40	42
	Independencia	15,668	4	3	12	10
	Los Olivos	19,666	4	4	16	51
	Puente Piedra	5791	1	14	14	13
	San Martín de Porres	20,881	4	7	28	28
	Santa Rosa	1958	0	1	0	0
Lima Sur	Chorrillos	9427	2	9	18	4
	Lurin	633	0	1	0	2
	Pachacamac	950	0	1	0	1
	Pucusana	556	0	1	0	0
	Punta Hermosa	196	0	1	0	0
	Punta Negra	67	0	1	0	0
	San Bartolo	206	0	1	0	0
	San Juan de Miraflores	17,606	4	8	32	9
	Santa María del Mar	123	0	1	0	0
	Villa María del Triunfo	12,188	2	14	28	5
Villa El Salvador	6359	4	7	28	9	

* National Census, 2017 [36].

In addition, this monitoring was carried out from 2016 to 2019, where, in some sampling dwellings, only one monitor was placed; it represented a single value of ^{222}Rn concentration. In the other sampling dwellings, where there was more than one monitor; the average ^{222}Rn concentration was taken into account.

2.3. Methods of Measurements

Indoor ^{222}Rn levels were measured by using LR-115 detectors in two modes: bare and diffusion chambers. Detectors in bare mode recorded the total radon concentration (^{222}Rn , ^{220}Rn , and their progeny), and two diffusion chambers—a commercial DPR monitor (ALGADE's laboratory, France) and a home-made plastic monitor, referred to hereafter as G2—registered ^{222}Rn level concentrations in air. The measurements were carried out using 508 bare detectors, as well as 140 G2 and 98 DPR monitors.

2.3.1. Bare LR-115 Detectors

Bare mode detectors are low-cost and easy-to-use. This exposure mode was employed for indoor measurements, where detectors were affixed onto a plastic plate and positioned on the walls at a height of roughly 1.5 m above the floor, with their sensitive surfaces facing the air.

It has been reported that concentrations of ^{232}Th are generally low in the building materials that are commonly used in Lima households [46]. However, even in walls with significant thorium content, ^{220}Rn exhalation may be reduced due to paint layers covering most studied dwellings. In any case, ^{220}Rn concentrations rapidly decrease with distance from the wall due to their short half-lives, which reach only about 10–15 cm from the wall under low ventilation rates [47]. This results in a reduction in ^{220}Rn concentration in its effective volume to around 25–30% of its value very close to the wall. Furthermore, given that most exhaled ^{220}Rn atoms decay in close proximity to the wall, it is anticipated that nearly all of their progeny will deposit on the wall before decaying in the air, except for ^{216}Po . Experimental findings have confirmed this approach, since a very low ^{220}Rn equilibrium factor was observed near the wall [48]. Therefore, a negligible contribution of the ^{220}Rn progeny to the detector track density is expected. In summary, the primary contribution to track density in the LR-115 bare detector placed on a wall is from ^{222}Rn and its non-equilibrated progeny. However, in cases of walls with high thorium content and a permeable paint layer, the ^{220}Rn contribution may be significant, especially considering its doubling due to the daughter ^{216}Po decaying practically at the same location and time as its parent.

If the interference of ^{220}Rn and its progeny can be considered negligible, the ^{222}Rn calibration factor for bare LR-115 detectors (K_B) will depend on the partial sensitivity for each species k_B and the ^{222}Rn equilibrium factor F_{Rn} , which can be expressed as [49]:

$$K_B = k_B \cdot (1 + 2 \cdot F_{Rn}) \quad (1)$$

By considering a partial sensitivity of $0.02 \text{ tracks} \cdot \text{cm}^{-2} \cdot \text{Bq}^{-1} \cdot \text{d}^{-1} \cdot \text{m}^3$ [50] and an equilibrium factor within the range of 0.2 to 0.7 [51], a mean calibration factor of $(0.038 \pm 0.005) \text{ tracks} \cdot \text{cm}^{-2} \cdot \text{Bq}^{-1} \cdot \text{d}^{-1} \cdot \text{m}^3$ was derived using an equilibrium factor of 0.45, where the lower and higher uncertainty limits were calculated using 0.2 and 0.7 respectively. This value closely matches the experimentally obtained calibration factor in our laboratory while taking into account their respective experimental uncertainties.

For the bare mode exposure, an LR-115 detector of size $15 \times 15 \text{ mm}^2$ was fixed to a plastic mica sheet; this ^{222}Rn monitor was mounted on an internal wall of the dwelling for measurements. Each volunteer was provided with an envelope containing two monitors of this type and an information guide on how to position them for measurements. Detectors were exposed for 8 to 12 weeks in different seasons according to previous studies [29], and research was carried out by us [52]. The lower limit of detection (LLD) was $15 \text{ Bq} \cdot \text{m}^{-3}$ [53].

2.3.2. Diffusion Chambers

The diffusion chamber of the G2 monitor is a cylindrical container composed of a white polypropylene double-walled container of 100 mL internal volume. A $1.5 \times 1.5 \text{ cm}^2$ LR-115 detector was fixed inside the chamber. It was expected that the double-wall design would mitigate the influence of environmental conditions, particularly air temperature. The ^{222}Rn and ^{220}Rn atoms enter the diffusion chamber through threads between the cup lid and the body chamber by diffusion. It was expected that, due to the short half-life of ^{220}Rn (55.6 s), a few atoms would enter the monitor and lead to a negligible ^{220}Rn concentration in its effective volume. The transmission factor was experimentally determined, and this hypothesis was confirmed. Therefore, the LR-115 placed inside the monitor only recorded alpha particles of ^{222}Rn and its progeny. A calibration factor of $(0.0238 \pm 0.0007) \text{ tracks} \cdot \text{cm}^{-2} \cdot \text{Bq}^{-1} \cdot \text{d}^{-1} \cdot \text{m}^3$ was used to convert the track density to ^{222}Rn concentration [54]. The exposure time of G2 monitors was approximately twelve weeks. LLD was expected to be approximately $20 \text{ Bq} \cdot \text{m}^{-3}$ [53].

Commercial DPR monitors were also used for ^{222}Rn monitoring. They were based on an LR-115 detector encapsulated in a sealed conductive plastic half-dome. The ^{222}Rn enters into the detection volume by diffusion through a specific membrane, which prevents ^{220}Rn , as well as radioactive aerosol particles, from entering and affecting the measurement. An OFF/ON system allows for the establishment of the measurement period. DPR recommends a minimum exposure period of two months for indoor measurements, which permits a ^{222}Rn activity of $20 \text{ Bq} \cdot \text{m}^{-3}$ to be measured properly [55]. DPR monitor was exposed during a period of approximately twelve weeks.

After exposure, DPR monitors were sent to ALGADE's laboratory for analysis, and results were reported with a global uncertainty of $\pm 2\sigma$. LR-115 detectors from bare and G2 monitors were etched at PUCP Nuclear Tracks Laboratory using a 2.5 N NaOH solution at a temperature of $60 \text{ }^\circ\text{C}$ for 90 min and rinsed using a magnetic stirrer. The track counting process of the LR-115 detectors was carried out with the POLITRACK reading system [Available online: <https://miam.it/prodotti/politrack/> (accessed on 7 May 2023)].

2.4. ^{222}Rn Concentration

The ^{222}Rn concentration in $\text{Bq} \cdot \text{m}^{-3}$ was calculated according to the following formula:

$$C_{i,Rn} = \frac{\rho}{K_i \cdot t} \quad i = B, G2 \quad (2)$$

where $C_{i,Rn}$ is the ^{222}Rn concentration ($\text{Bq} \cdot \text{m}^{-3}$), ρ is the effective track density ($\text{tracks} \cdot \text{cm}^{-2}$) that is calculated by subtracting the background density from the total density, t is the exposure time (days), and K_i is the calibration factor for the bare (B) detector or diffusion chamber G2 (G2).

2.5. Statistical Treatment of Data and Mapping

Indoor ^{222}Rn concentration often exhibits a skewed distribution with a long tail to the right, and log-normal distribution is usually used to model it [56]. The Anderson–Darling test was applied to evaluate the normal distribution of the logarithmically transformed data. The analysis of variance (ANOVA) was utilized to make comparisons between the four defined zones and other variables. The OriginPro 2023b software was employed.

The inverse distance weighted (IDW) interpolation model was utilized to map ^{222}Rn concentrations. IDW interpolation is based on the principle that nearby measured points have a stronger influence on the estimation of unknown values. This method calculates a weighted combination of known points, where the weight is a function of the inverse distance. To predict a value for an unmeasured location, IDW takes into account the measured values surrounding the prediction location. Points closer to the prediction location are given greater importance than those farther away [57].

Another powerful interpolation is the Kriging model, which can also be effectively utilized to map ^{222}Rn concentration levels. By employing Kriging, we can create accurate

and detailed maps of ²²²Rn concentration, because it takes into account the spatial autocorrelation of ²²²Rn data, thereby capturing the relationship between nearby measurements and generating predictions for unobserved locations. This model also considers both the observed data and the underlying spatial structure, which results in reliable estimates of ²²²Rn levels throughout the study area [58].

Both models were implemented by using ArcGISPro 2022 software.

3. Results and Discussion

3.1. Results for Bare Detectors

The distribution of indoor ²²²Rn concentration is typically skewed, and the logarithmic transformation can be useful for assessing the risk of exposure to ²²²Rn. Figure 2a depicts the indoor ²²²Rn concentration distribution. As anticipated, the indoor ²²²Rn concentrations followed a log-normal distribution (shown by the continuous line in figure Figure 2a). The Q–Q plot in Figure 2b represents the natural log-transformed ²²²Rn concentration, which followed the expected trend. The Anderson–Darling test, with a 95% confidence level, suggests that the observed distribution matches a normal distribution, since the *p*-value is greater than 0.05. Approximately 2.27% of the measurements exceeded the reference level of 200 Bq·m⁻³ established by IPEN.

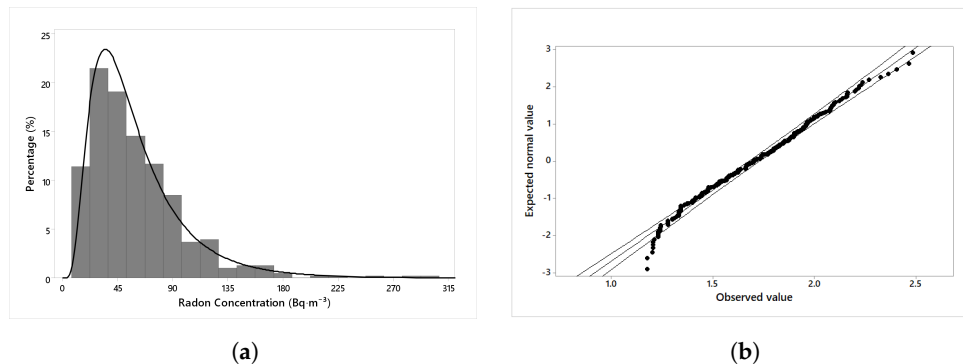


Figure 2. (a) Log–normal distribution of the indoor ²²²Rn concentration. (b) Q–Q plot of natural log-transformed ²²²Rn concentration.

Basic descriptive statistical parameters and other parameters such as the geometric mean (GM), geometric standard deviation (GSD), minimum (Min), maximum (Max), median, population density, and number of dwellings are reported in Table 3. In addition, the ANOVA analyses are listed in Table 3.

Table 3. Descriptive statistical results and ANOVA analysis of the indoor ²²²Rn concentration obtained using bare detectors by zones.

Variables	Number of Dwellings	Population Density per km ²	Min (Bq·m ⁻³)	Max (Bq·m ⁻³)	Median (Bq·m ⁻³)	GM (Bq·m ⁻³)	GSD (Bq·m ⁻³)	ANOVA			
								F-Value	<i>p</i> -Value	Percentage of Variation (%)	
Zones	Lima Centro	235	14,588	16	306	63	57	2			69.24
	Lima Este	58	13,226	16	228	39	39	2	8.57659	0.00002	8.90
	Lima Norte	110	11,278	16	166	45	45	2			17.67
	Lima Sur	34	4188	15	133	34	37	2			4.19

The average ²²²Rn concentration in the total number of dwellings using bare detectors was (49 ± 2) Bq·m⁻³. This value is above the world average 39 Bq·m⁻³, but below the WHO recommended reference level of 100 Bq·m⁻³ [29]. We also determined that the values of the bare monitor in 5% of the measured dwellings were lower than the detection limit.

Table 3 also shows the ANOVA analysis on the ^{222}Rn concentration data for different zones. In this case, the obtained F-value indicates that there were differences in ^{222}Rn concentration between the zones, and the small p-value suggests that these differences are statistically significant. Therefore, we can infer that the zone has a significant impact on the ^{222}Rn concentration, and these findings can be attributed to unique factors associated with each specific zone, including the geological characteristics commonly examined in previous studies [34]. Additionally, Ref. [34] also identified high levels of ^{222}Rn concentrations near alluvial deposits such as Lima Centro, which potentially corroborates the findings obtained in this study.

In this study, we also analyzed the ^{222}Rn concentration related to the construction age, vehicular traffic, construction materials, wall painting, and floor type, as shown in Table 4.

Basic descriptive statistical results from Table 4 suggest that different variables were associated with higher levels of ^{222}Rn in dwellings. For instance, dwellings over 40 years old had the highest GM of ^{222}Rn concentration, which may be due to the fact that older dwellings are more likely to have cracks and other openings that can allow ^{222}Rn to enter. Similarly, dwellings located near highways may have higher ^{222}Rn levels due to the high vehicular traffic that produces vibrations leading to larger ^{222}Rn exhalations from soils [59]. In the construction materials group, we found that dwellings with other materials had a slightly higher ^{222}Rn concentration. It suggests that, for wall painting, the dwellings with older wall painting had higher ^{222}Rn concentrations. This finding is connected to the fact that older painting may have become worn or damaged over time, thereby no longer providing a barrier to prevent the ^{222}Rn exhalation from walls. Finally, the tapestry had higher concentrations, because it has more porosity compared to more dense materials such as cement.

On the other hand, ANOVA analyses suggest that only the construction age variable showed a statistically significant effect on the ^{222}Rn concentration. This could indicate that cracks and other openings that can allow ^{222}Rn to enter due to the construction age are statistically significant factors, as previous studies have also observed a correlation between indoor radon concentration and the presence of cracks [60].

3.2. Results for Diffusion Chambers

The ^{222}Rn concentration measured with G2 monitors inside dwellings from September 2017 to December 2018 gave a mean value of $(66 \pm 2) \text{ Bq}\cdot\text{m}^{-3}$. In addition, it was determined that 40.7% of the measurement dwellings presented values lower than the detection limit of the G2 monitor ($<20 \text{ Bq}\cdot\text{m}^{-3}$), and 6.4% gave values within the range of the level of action for chronic exposure to ^{222}Rn in dwellings ($200\text{--}600 \text{ Bq}\cdot\text{m}^{-3}$) indicated in the Peruvian National Regulation of Radiological Safety (D.S. No. 009-97-EM) [33]. The distribution of the obtained values is presented by means of a histogram in Figure 3. Results of the statistical parameters of indoor ^{222}Rn concentration are shown in Table 5.

Apparently, high humidity conditions and temperature changes are known to potentially cause condensation at 95% humidity and a temperature of $23\text{ }^{\circ}\text{C}$. In certain months, the humidity in Lima reaches 99%, which could have caused this effect (citation), along with condensation effects and the dew point [61]. This would mainly affect the filtering membrane of the DPRs, as the manufacturer recommends avoiding condensation. Another possible factor that could have affected the response of the DPR membrane was the high particulate matter in the city of Lima [62], which would have hindered the proper functioning of the filtering membrane. In the case of the G2 monitors, their double-walled structure with thermal insulation effects may have helped reduce the influence of condensation and allow the passage of ^{222}Rn without major issues.

Table 4. Descriptive statistical results and ANOVA analysis of the indoor ²²²Rn concentration using bare detectors for some variables.

Variables		Number of Dwellings	Min (Bq·m ⁻³)	Max (Bq·m ⁻³)	Median (Bq·m ⁻³)	GM (Bq·m ⁻³)	GSD (Bq·m ⁻³)	ANOVA		
								F-Value	p-Value	Percentage of Variation (%)
Construction Age (years)	0 to 20	195	15	255	50	50	2	4.58541	0.01082	45.99
	20 to 39	78	15	166	50	48	2			16.90
	Over 40	82	16	306	64	59	2			37.12
Vehicular Traffic	Low	240	15	306	50	51	2	0.25429	0.77559	65.81
	Medium	124	16	232	50	50	2			28.95
	High	25	24	145	55	54	2			5.24
Construction Materials	Bricks	335	15	306	50	51	2	0.20569	0.81417	87.75
	Adobe	10	16	145	37	43	2			2.55
	Others	32	17	232	55	54	2			9.70
Wall Painting (years)	Over 5	108	15	212	53	52	2	2.03990	0.154371	44.62
	Below 5	165	16	255	49	49	2			55.38
Floor Type *	Cement	99	15	292	46	49	2	0.07429	0.98995	27.78
	Wood	65	16	306	50	51	2			20.27
	Majolica	146	16	255	54	51	2			36.31
	Tapestry	12	16	125	64	53	2			2.95
	Others	55	18	186	55	51	2			12.69

* All detectors were placed on first level.

Table 5. Descriptive statistical results and ANOVA analyses of the indoor ²²²Rn concentration using G2 monitors by zones.

Variables		Number of Dwellings	Min (Bq·m ⁻³)	Max (Bq·m ⁻³)	Median (Bq·m ⁻³)	GM (Bq·m ⁻³)	GSD (Bq·m ⁻³)	ANOVA		
								F-Value	p-Value	Percentage of Variation (%)
Zones	Lima Centro	23	25	306	109	94	2	1.98629	0.12255	37.39
	Lima Este	31	20	292	72	67	2			34.55
	Lima Norte	17	20	235	64	67	2			19.98
	Lima Sur	14	22	208	37	45	2			8.08

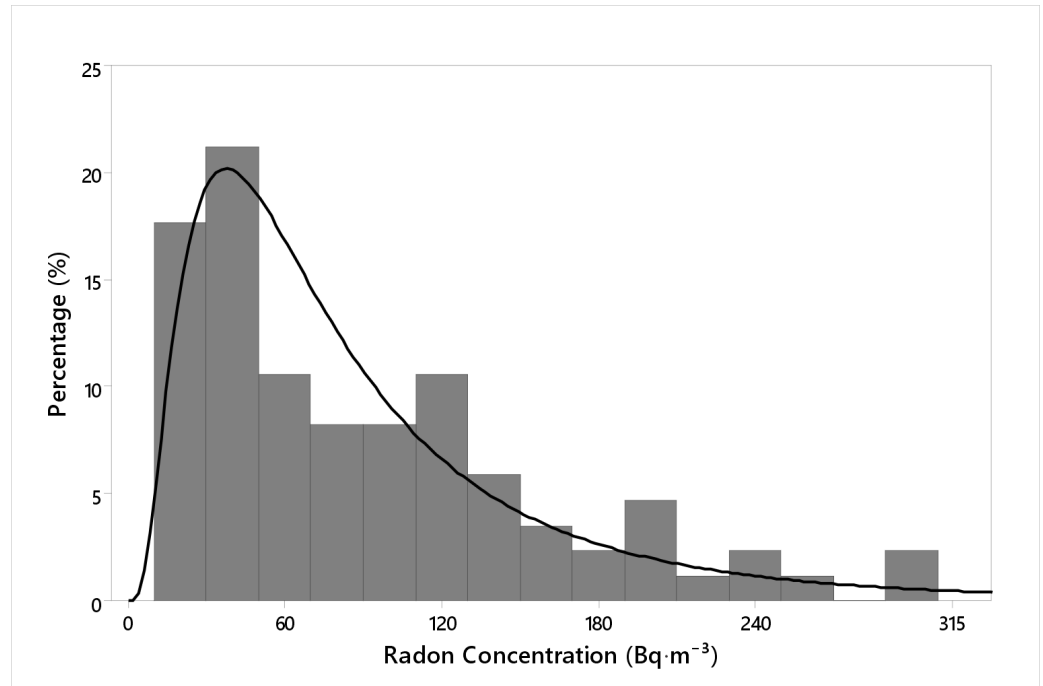


Figure 3. ²²²Rn concentration distribution using the G2 monitors.

Based on the findings of our study, it is evident that the ALGADE monitors did not perform optimally under the high air humidity conditions of Lima province. Only five monitors (<6%) yielded results above their detection limit of 20 Bq·m⁻³ [63]; therefore, the results obtained with ALGADE monitors were not considered for the analysis and interpretation data. These findings underscore the importance of carefully selecting monitoring equipment that is capable of reliably and accurately measuring environmental parameters under a wide range of local conditions. As such, it is imperative that future efforts are directed towards developing technologies that can withstand ‘extreme’ conditions and provide accurate data for informed decision making.

3.3. Comparing the Bare Mode Detector and the G2 Monitor Results

The average ²²²Rn concentration per zone using bare mode detectors and G2 monitors is depicted in Figure 4.

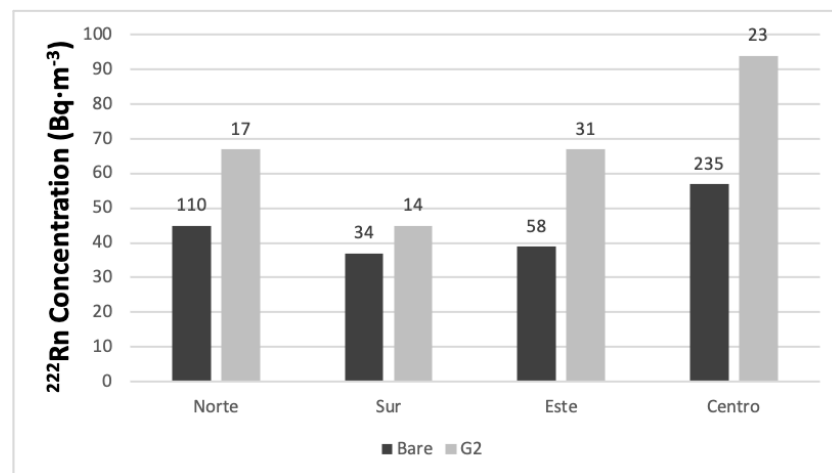


Figure 4. Comparing average ²²²Rn concentrations per zone obtained by using the bare mode and the G2 monitor. The numbers of dwellings are displayed above the bars.

The results were compared, and we found that the ^{222}Rn concentrations measured by G2 monitors were higher than those obtained by bare mode detectors. The G2 monitor measurements showed a range of (45 ± 7) to (94 ± 8) $\text{Bq}\cdot\text{m}^{-3}$, whereas the average bare mode detector values ranged from (37 ± 5) to (57 ± 7) $\text{Bq}\cdot\text{m}^{-3}$.

In order to evaluate the statistical difference between both bare mode and G2 monitor, the Mann–Whitney U test was used. The results of this test indicate that both modes were significantly different ($p = 0.0004$) with a 95% confidence level. These results may be due to two reasons: either the ^{220}Rn and its progeny contributed to the density of tracks recorded in the bare detector, or the assumed equilibrium factor was higher than the actual value. These factors should be taken into account in future investigations.

Therefore, it can also be concluded that the average ^{222}Rn concentrations in both cases were below the reference level ($200 \text{ Bq}\cdot\text{m}^{-3}$) established by the IPEN. Besides, the contributions of ^{220}Rn and its progeny to the track density detected in the exposed bare mode detectors were low. As such, any subsequent assessments of inhalation dose estimations should take this into account. Another possible cause of the fact that the concentrations measured with the bare monitors were consistently lower than those obtained with the G2 monitors is that the actual equilibrium factor may have been lower than the assumed value used to calculate the calibration factor using Equation (1).

3.4. ^{222}Rn Map in Lima

This section discusses the ^{222}Rn map of Lima province, which is a visual representation of the ^{222}Rn levels. The map is based on data from ^{222}Rn measurements taken in various locations throughout Lima province using bare mode outcomes. This map represents an important tool for identifying areas of high ^{222}Rn levels, which can pose a health risk to the residents of the Lima province. According to this and depending on the high ^{222}Rn level, there are various mitigation methods to control those levels. Thus, color ^{222}Rn maps indicating the indoor ^{222}Rn levels in the Lima province were elaborated using IDW and the Kriging model. Both results are shown in Figures 5 and 6, respectively. These interpolation models use measurement results of the ^{222}Rn concentration in known locations to estimate the ^{222}Rn concentration in locations where no measurements have been taken.

The ranges of ^{222}Rn concentrations required to obtain the map vary depending on the regulations and recommendations of each country or public health authority. In this study, the following ranges were used [64–67]:

- Low: less than $50 \text{ Bq}\cdot\text{m}^{-3}$;
- Moderate: between 50 and $100 \text{ Bq}\cdot\text{m}^{-3}$;
- High: between 100 and $200 \text{ Bq}\cdot\text{m}^{-3}$;
- Very high: greater than $200 \text{ Bq}\cdot\text{m}^{-3}$.

In Figures 5 and 6, the legend on the right side of the map shows the color codes and the corresponding ^{222}Rn levels in $\text{Bq}\cdot\text{m}^{-3}$, and the ^{222}Rn concentration results represent the mean value. In the Lima Sur zone, both models depict that the distribution was clearly lower than $100 \text{ Bq}\cdot\text{m}^{-3}$, while the Lima Centro zone depicts the highest ^{222}Rn levels. It should be emphasized that, although the map results confirmed the trend of the statistical data analysis, they allow the spatial visualization of the ^{222}Rn levels of each zone.

The cross-validation results for the IDW and Kriging models indicate that neither model provided a good fit to the residential ^{222}Rn concentration data, as shown in Table 6. Both models presented negative values of R^2 , which indicates that the model could not well explain the variability in the data. Furthermore, the MAE, RMSE, and RMS values indicate that both models have a high error in the prediction of the ^{222}Rn concentration. A possible explanation for these results is that the density of measurements was not uniform throughout the study area. That is, some areas may have had more measurements than others, which may have affected the accuracy of the models. For example, if there are areas with fewer measurements, the model may have difficulty estimating the ^{222}Rn concentration in those areas. Therefore, the models could be improved if more measurements are made

in the whole study area. It should be noted that these results are preliminary, and further measurements are needed to fully assess the accuracy of the IDW and Kriging models. In addition, there are other factors, such as geology and soil characteristics, that can also affect the ^{222}Rn concentration and must be considered in modeling. Therefore, it is recommended to continue taking measurements and improving the models to provide a more accurate map of the ^{222}Rn concentration in the study area.

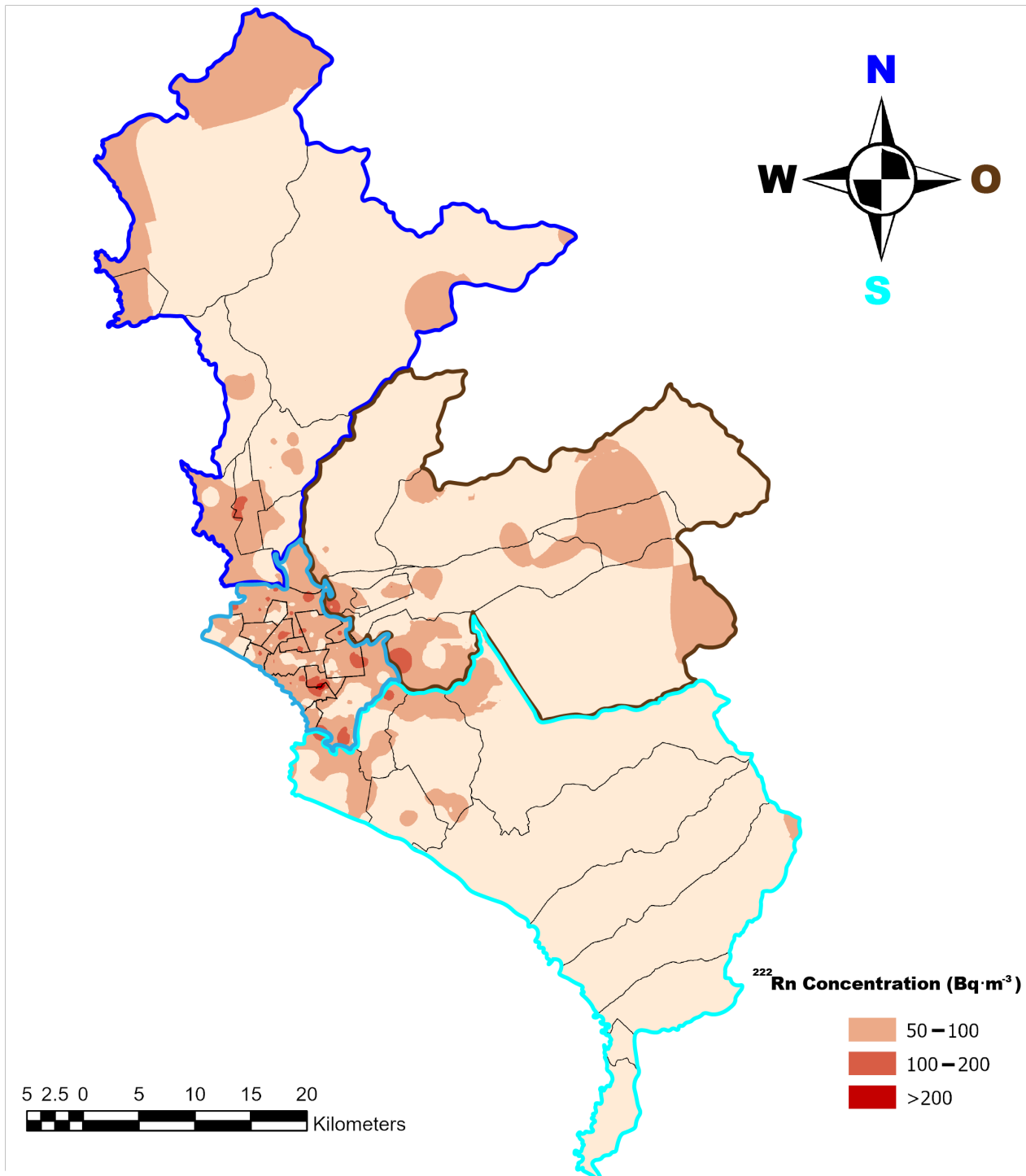


Figure 5. Indoor ^{222}Rn map of Lima province using the IDW model.

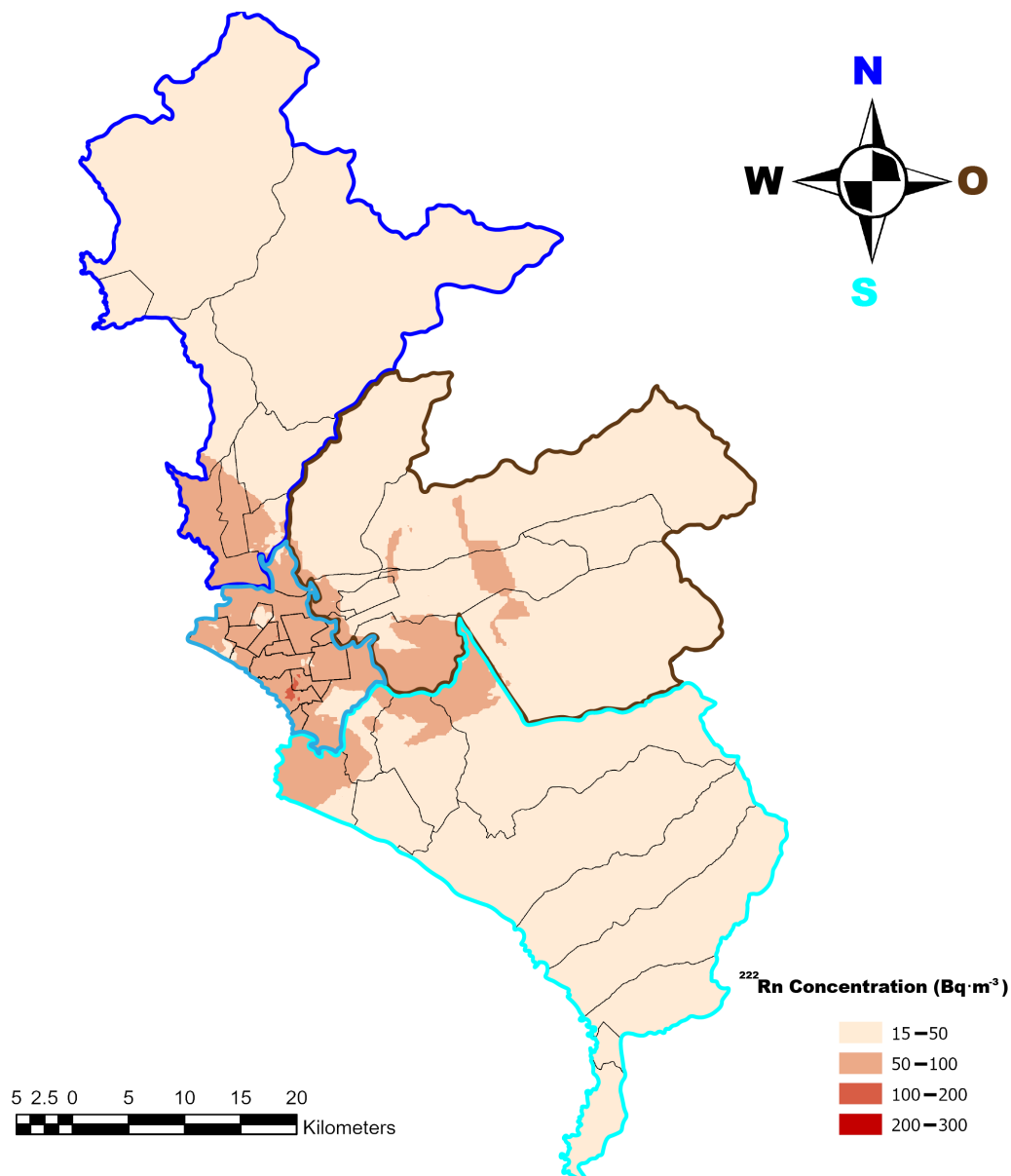


Figure 6. Indoor ^{222}Rn map of Lima province using the Kriging model.

Table 6. The cross-validation results for the IDW and Kriging models.

Method	MAE *	RMS *	RMSE *	R ²
IDW	36.358	4.971	49.546	−0.637
Kriging	32.451	41.474	43.856	−0.240

* MAE is the mean absolute error; RMS is the root mean square; and RMSE is the root mean square error.

The indoor ^{222}Rn map of Lima is not a finalized map, and it will be improved when new measurement data is obtained.

4. Conclusions

Indoor ^{222}Rn concentrations were measured in 508 dwellings using 508 bare detectors. Simultaneously and randomly, in 140 and 98 of them, G2 and DPR monitors were used, respectively. Using bare mode, the geometric mean was $49 \text{ Bq}\cdot\text{m}^{-3}$ and, for the G2 diffusion chambers, the GM was $66 \text{ Bq}\cdot\text{m}^{-3}$; both of them were under the action level. In the case of bare detectors, 88.98% of the devices recorded measurements below $100 \text{ Bq}\cdot\text{m}^{-3}$, which includes those that reported values below the detection limit. A total of 9.84% of

the detectors registered measurements between 100 and 200 Bq·m⁻³, while only 1.18% registered concentrations above 200 Bq·m⁻³.

On the other hand, in the case of the G2 monitors, 63.05% of the devices recorded measurements below 100 Bq·m⁻³. A total of 7.17% of the monitors recorded measurements between 100 and 200 Bq·m⁻³, while only 9.78% of the monitors recorded values above 200 Bq·m⁻³. Most of the ²²²Rn concentration results reported by the ALGADE laboratory were below the DPR's detection limit.

Bare detectors follow a log normal distribution, which are in contrast to G2 diffusion chamber distributions; this is due to the low number of measurements. From the results obtained by measuring ²²²Rn concentrations using bare detectors and G2 detectors, we can infer that bare detectors mainly register the contribution of ²²²Rn, with the contribution of ²²⁰Rn and its progenies are recorded as negligible. In the case of G2 detectors, they register the concentration of ²²²Rn and the progeny that is produced inside the chamber, and they meet the requirements of the critical angle and appropriate energy range to produce tracks.

The concentration of ²²²Rn was closely related to the zones, as evidenced by the strong correlation with the geological characteristics. It was also evidently related to other variables such as the construction age. This factor seems to indicate that the proper maintenance of dwellings (without cracks or fissures) contributes to lower levels of ²²²Rn inside dwellings.

The first ²²²Rn map in Peru, specifically in its capital Lima, has been created. Although the results are not conclusive, it can be said that the detected levels do not pose a high risk to the population, since the average ²²²Rn concentration values for both exposure modes were below the reference level suggested by WHO. Further measurements are necessary to study other regions. These findings highlight the importance of monitoring indoor ²²²Rn levels and implementing proper dwelling maintenance practices to reduce exposure.

Based on the obtained results, it is evident that LR-115 detectors, whether used in a bare mode or diffusion chamber mode, exhibit good performance and can be employed in this type of study, given their low-cost and ease-of-use. They are suitable for laboratories conducting research on related topics.

Author Contributions: Conceptualization, P.P., M.E.L.-H. and D.P.F.; methodology, P.P., M.E.L.-H., L.V.L. and D.P.F.; software, B.P., J.R. and R.L.; validation, L.S.-B., B.P., J.R. and C.J.G.-P.; formal analysis, P.P., D.P.F., L.S.-B., B.P., J.R. and R.L.; investigation, P.P., M.E.L.-H., D.P.F., C.J.G.-P. and L.V.L.; writing—original draft preparation, P.P. and M.E.L.-H.; writing—review and editing, D.P.F., B.P., J.R., C.J.G.-P., R.L. and L.S.-B.; supervision, P.P., M.E.L.-H., D.P.F. and S.G.; project administration, P.P.; funding acquisition, P.P. and S.G. All authors have read and agreed to the published version of the manuscript.

Funding: This research was funded by INNOVATE PERU, grant number 120-PNICP-PIAP-2015 (“Desarrollo de un sistema de monitoreo de Rn-222 ambiental mediante la técnica de huellas nucleares, en la ciudad de Lima, Perú”); by the IAEA, grant number PER 9024 (“Radon levels in dwellings in three regions of Peru and creating radon maps for policy makers”); and by CienciActiva-CONCYTEC 2017. We also express gratitude to Departamento de Ciencias—PUCP for funding the open access option for our paper publication.

Institutional Review Board Statement: Not applicable.

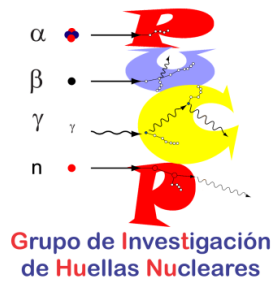
Informed Consent Statement: Not applicable.

Data Availability Statement: The data that support the findings of this study are available from the corresponding author (P.P.) upon reasonable request.

Acknowledgments: All the authors would like to express their gratitude to the community university, to the volunteers who allowed this work to be carried out, and to IAEA for technical support.

Conflicts of Interest: The authors declare no conflict of interest. The funders had no role in the design of the study; in the collection, analyses, or interpretation of data; in the writing of the manuscript, or in the decision to publish the results.

Appendix A



Ficha de Ubicación Detector de Rn 222

Responsable:

Código de los detectores

--	--

Datos Generales:

Dirección					
Distrito			Teléfono		
Edad aprox. de la construcción (años)		Número Habitantes		Número Fumadores:	
La casa está en:	avenida	calle	Interior o pasaje		
El tráfico es:	intenso	medio	bajo		
Transitan mayormente:	Pesados (ómnibus y camiones)		Livianos (autos)		
En los alrededores hay:	Fábricas con emisión de gases	Fábrica sin emisión de gases	Cables de alta tensión	aeropuerto	

Características del lugar de monitoreo

sala	cocina	dormitorio	baño	Garaje	
Sótano	semisótano	Primer piso	Segundo piso	otro	
¿Fuman en la habitación?			si	no	
¿Tiene ventana(s)?			si	no	
¿Quedan abiertas?	siempre	nunca	En el día	Por la noche	Por horas
¿Otro sistema?	Ventilador de techo	Aire acondicionado	Extractor de aire	otro	Nada
El sistema adicional está prendido	siempre	nunca	Solo de día	Solo de noche	Por momentos
Material de construcción		ladrillos	adobe	drywall	otros
Recubrimiento	pintura	madera	papel	mayólica	otros

References

1. UNSCEAR. *Sources and Effects of Ionizing Radiation, United Nations Scientific Committee on the Effects of Atomic Radiation (UNSCEAR) 2000 Report, Volume I: Report to the General Assembly, with Scientific Annexes-Sources*; United Nations: New York, NY, USA, 2000.
2. Bochicchio, F. The radon issue: Considerations on regulatory approaches and exposure evaluations on the basis of recent epidemiological results. *Appl. Radiat. Isot.* **2008**, *66*, 1561–1566. [[CrossRef](#)] [[PubMed](#)]
3. Nikezic, D.; Yu, K. Are radon gas measurements adequate for epidemiological studies and case control studies of radon-induced lung cancer? *Radiat. Prot. Dosim.* **2005**, *113*, 233–235. [[CrossRef](#)] [[PubMed](#)]
4. Ramola, R.; Choubey, V.; Negi, M.; Prasad, Y.; Prasad, G. Radon occurrence in soil–gas and groundwater around an active landslide. *Radiat. Meas.* **2008**, *43*, 98–101. [[CrossRef](#)]
5. National Research Council (US) Committee on Health Risks of Exposure to Radon (BEIR VI). *The Health Effects of Exposure to Indoor Radon. Biological Effects of Ionizing Radiation*; United Nations: New York, NY, USA, 1998.
6. WHO. *Protection of the Public against Exposure Indoors Due to Radon and Other Natural Sources of Radiation. Specific Safety Guide*; WHO: Geneva, Switzerland, 2015.
7. UNSCEAR. *Effects of Ionizing Radiation, United Nations Scientific Committee on the Effects of Atomic Radiation (UNSCEAR) 2006 Report, Volume I: Report to the General Assembly, Scientific Annexes A and B*; United Nations: New York, NY, USA, 2008.
8. Lowder, W.M. Natural environmental radioactivity and radon gas. In *Radon Monitoring in Radioprotection, Environmental Radioactivity and Earth Sciences*; World Scientific: Singapore, 1990.
9. Brenner, D. *Protection against Radon-222 at Home and at Work. ICRP Publication 65*; SAGE Publications Ltd.: Thousand Oaks, CA, USA, 1994.
10. Shakir Khan, M.; Zubair, M.; Verma, D.; Naqvi, A.; Azam, A.; Bhardwaj, M. The study of indoor radon in the urban dwellings using plastic track detectors. *Environ. Earth Sci.* **2011**, *63*, 279–282. [[CrossRef](#)]
11. Rafique, M.; Rahman, S.; Rahman, S.; Jabeen, S.; Shahzad, M.I.; Rathore, M.H. Indoor radon concentration measurement in the dwellings of district Poonch (Azad Kashmir), Pakistan. *Radiat. Prot. Dosim.* **2010**, *138*, 158–165. [[CrossRef](#)]
12. Da Silva, N.; Bossew, P. The planned Brazilian indoor radon survey-concepts and particular challenges. *Radiat. Prot. Dosim.* **2014**, *162*, 105–109. [[CrossRef](#)]
13. Espinosa, G.; Golzarri, J.; Chavarria, A.; Castaño, V. Indoor radon measurement via Nuclear Track Methodology: A comparative study. *Radiat. Meas.* **2013**, *50*, 127–129. [[CrossRef](#)]
14. Tollefsen, T.; Cinelli, G.; Bossew, P.; Gruber, V.; De Cort, M. From the European indoor radon map towards an atlas of natural radiation. *Radiat. Prot. Dosim.* **2014**, *162*, 129–134. [[CrossRef](#)]
15. Poncela, L.Q.; Fernández, P.; Arozamena, J.G.; Sainz, C.; Fernández, J.; Mahou, E.S.; Matarranz, J.M.; Cascón, M. Natural gamma radiation map (MARNA) and indoor radon levels in Spain. *Environ. Int.* **2004**, *29*, 1091–1096. [[CrossRef](#)]
16. National Research Council. *Health Risks of Radon and Other Internally Deposited Alpha-Emitters: BEIR IV*; National Academies Press: Washington, DC, USA, 1988.
17. Dubois, G. *An Overview of Radon Surveys in Europe*; European Commission: Brussels, Belgium, 2005; pp. 1–168.
18. WHO. *International Radon Project: Survey on Radon Guidelines, Programmes and Activities*; Technical Report; World Health Organization: Geneva, Switzerland, 2007.
19. Pantelić, G.; Čeliković, I.; Živanović, M.; Vukanac, I.; Nikolić, J.; Cinelli, G.; Gruber, V. *Literature Review of INDOOR Radon Surveys in Europe*; Publications Office of the European Union: Luxembourg, 2018. [[CrossRef](#)]
20. Serge Didier, T.S.; Saïdou, Tokonami, S.; Hosoda, M.; Suzuki, T.; Kudo, H.; Bouba, O. Simultaneous measurements of indoor radon and thoron and inhalation dose assessment in Douala City, Cameroon. *Isot. Environ. Health. Stud.* **2019**, *55*, 499–510. [[CrossRef](#)]
21. Sabbarese, C.; Ambrosino, F.; Roca, V. Analysis by scanner of tracks produced by radon alpha particles in CR-39 detectors. *Radiat. Prot. Dosim.* **2020**, *191*, 154–159. [[CrossRef](#)]
22. Loffredo, F.; Savino, F.; Amato, R.; Irollo, A.; Gargiulo, F.; Sabatino, G.; Serra, M.; Quarto, M. Indoor radon concentration and risk assessment in 27 districts of a public healthcare company in Naples, South Italy. *Life* **2021**, *11*, 178. [[CrossRef](#)]
23. Loffredo, F.; Opoku-Ntim, I.; Meo, G.; Quarto, M. Indoor Radon Monitoring in Kindergarten and Primary Schools in South Italy. *Atmosphere* **2022**, *13*, 478. [[CrossRef](#)]
24. Hansen, V.; Petersen, D.; Søgaard-Hansen, J.; Rigét, F.F.; Mosbech, A.; Clausen, D.S.; Mulvad, G.; Rönnqvist, T. Indoor radon survey in Greenland and dose assessment. *J. Environ. Radioact.* **2023**, *257*, 107080. [[CrossRef](#)]
25. Ramachandran, T.; Eappen, K.; Shaikh, A.; Mayya, Y. Indoor radon levels and equilibrium factors in Indian dwellings. *Radiat. Prot. Environ.* **2001**, *24*, 420–422.
26. Singh, S.; Mehra, R.; Singh, K. Seasonal variation of indoor radon in dwellings of Malwa region, Punjab. *Atmos. Environ.* **2005**, *39*, 7761–7767. [[CrossRef](#)]
27. Virk, H. Indoor radon levels near the radioactive sites of Himachal Pradesh, India. *Environ. Int.* **1999**, *25*, 47–51. [[CrossRef](#)]
28. Pantelić, G.; Čeliković, I.; Živanović, M.; Vukanac, I.; Nikolić, J.K.; Cinelli, G.; Gruber, V. Qualitative overview of indoor radon surveys in Europe. *J. Environ. Radioact.* **2019**, *204*, 163–174. [[CrossRef](#)]
29. WHO. *WHO Handbook on Indoor Radon: A Public Health Perspective*; World Health Organization: Geneva, Switzerland, 2009.
30. Mayya, Y.; Eappen, K.; Nambi, K. Methodology for mixed field inhalation dosimetry in monazite areas using a twin-cup dosimeter with three track detectors. *Radiat. Prot. Dosim.* **1998**, *77*, 177–184. [[CrossRef](#)]

31. Omori, Y.; Tokonami, S.; Sahoo, S.K.; Ishikawa, T.; Sorimachi, A.; Hosoda, M.; Kudo, H.; Pornnumpa, C.; Nair, R.R.K.; Jayalekshmi, P.A.; et al. Radiation dose due to radon and thoron progeny inhalation in high-level natural radiation areas of Kerala, India. *J. Radiol. Prot.* **2016**, *37*, 111. [CrossRef]
32. Pérez, B.; López, M.; Palacios, D. Concentric rings formation on etched LR-115 in bare mode by unconventional exposition. *Nucl. Instrum. Methods Phys. Res. B* **2021**, *496*, 37–44. [CrossRef]
33. IPEN. Reglamento de Seguridad Radiológica. Available online: https://www.ipen.gov.pe/transparencia/regulacion/normatividad/ds009_97em.pdf (accessed on 8 May 2023).
34. Vilcapoma, L.L.; López Herrera, M.E.; Pereyra, P.; Palacios, D.F.; Pérez, B.; Rojas, J.; Sajo-Bohus, L. Measurement of radon in soils of Lima City-Peru during the period 2016–2017. *Earth Sci. Res. J.* **2019**, *23*, 171–183. [CrossRef]
35. Mapa de Lima. Mapa de las Regiones de la Provincia de Lima. Available online: <https://www.mapadelima.com/mapa-de-regiones-de-lima/> (accessed on 11 March 2023).
36. INEI. Resultados Definitivos de los Censo Nacionales 2017. Available online: https://www.inei.gov.pe/media/MenuRecursivo/publicaciones_digitales/Est/Lib1583/ (accessed on 7 May 2023).
37. INGEMMET. *Carta Geológica Nacional—501 Cuadrángulos Geológicos Digitales de la Carta Nacional 1960–1999*; INGEMMET: Lima, Peru, 1999.
38. Martínez-Martínez, J. Determinación de Procesos Litorales en Playas de Arena, Según el Contraste de los Valores Granulométricos. *Boletín. Instituto Español de Oceanografía* **1986**, *3*, 17–22. <https://accedacris.ulpgc.es/bitstream/10553/957/2/3836.pdf>.
39. MINSA. Estadística Poblacional. Available online: https://www.minsa.gov.pe/reunis/data/poblacion_estimada.asp (accessed on 11 March 2023).
40. Peel, M.C.; Finlayson, B.L.; McMahon, T.A. Updated world map of the Köppen-Geiger climate classification. *Hydrol. Earth Syst. Sci.* **2007**, *11*, 1633–1644. [CrossRef]
41. SENAMHI. Mapa Climático del Perú. Available online: <https://www.senamhi.gov.pe/?p=mapa-climatico-del-peru> (accessed on 24 March 2023).
42. CSN. Mapa de Zonificación por Municipio de Radón. Available online: <https://www.csn.es/mapa-de-zonificacion-por-municipio> (accessed on 11 March 2023).
43. Elío, J.; Crowley, Q.; Scanlon, R.; Hodgson, J.; Zgaga, L. Estimation of residential radon exposure and definition of Radon Priority Areas based on expected lung cancer incidence. *Environ. Int.* **2018**, *114*, 69–76. [CrossRef] [PubMed]
44. Murphy, P.; Dowdall, A.; Long, S.; Curtin, B.; Fenton, D. Estimating population lung cancer risk from radon using a resource efficient stratified population weighted sample survey protocol—Lessons and results from Ireland. *J. Environ. Radioact.* **2021**, *233*, 106582. [CrossRef]
45. Chen, J. A preliminary design of a radon potential map for Canada: A multi-tier approach. *Environ. Earth Sci.* **2009**, *59*, 775–782. [CrossRef]
46. IAEA Unveils Unique World Uranium Map. Available online: <https://www.iaea.org/newscenter/news/iaea-unveils-unique-world-uranium-map> (accessed on 3 April 2023).
47. Mishra, R.; Joshi, M.; Meisenberg, O.; Gierl, S.; Prajith, R.; Kanse, S.; Rout, R.; Sapra, B.; Mayya, Y.; Tschiersch, J. Deposition and spatial variation of thoron decay products in a thoron experimental house using the Direct Thoron Progeny Sensors. *J. Radiol. Prot.* **2017**, *37*, 379. [CrossRef]
48. Mishra, R.; Zunic, Z.S.; Venoso, G.; Bochicchio, F.; Stojanovska, Z.; Carpentieri, C.; Prajith, R.; Sapra, B.; Mayya, Y.; Ishikawa, T.; et al. An evaluation of thoron (and radon) equilibrium factor close to walls based on long-term measurements in dwellings. *Radiat. Prot. Dosim.* **2014**, *160*, 164–168. [CrossRef]
49. Eappen, K.; Mayya, Y. Calibration factors for LR-115 (type-II) based radon thoron discriminating dosimeter. *Radiat. Meas.* **2004**, *38*, 5–17. [CrossRef]
50. Eappen, K.; Ramachandran, T.; Mayya, Y.; Nambi, K. LR-115 detector response to alpha energies above 5.0 MeV: Application to thoron dosimetry. In Proceedings of the Seventh National Symposium on Environment, Dhanbad, India, 5–7 February 1998.
51. UNSCEAR. *Sources and Effects of Ionizing Radiation, United Nations Scientific Committee on the Effects of Atomic Radiation (UNSCEAR) 2006 Report, Report. Sources to Effects Assessment for Radon in Homes and Workplaces, vol. II (Annex E)*; United Nations: New York, NY, USA, 2009.
52. Canoba, A.; Lopez, F.; Arnaud, M.; Oliveira, A.; Neman, R.; Hadler, J.; Iunes, P.; Paulo, S.; Osorio, A.; Aparecido, R.; et al. Indoor radon measurements and methodologies in Latin American countries. *Radiat. Meas.* **2001**, *34*, 483–486. [CrossRef]
53. Belgaid, M.; Amrani, D. Investigations and Use of LR-115 Track Detectors for Radon Measurements. Czech Republic. July 2004. Available online: <https://www.osti.gov/etdeweb/servlets/purl/20555909> (accessed on 3 April 2023).
54. Pérez, B.; López, M.; Palacios, D. Theoretical and experimental study of the LR-115 detector response in a non-commercial radon monitor. *Appl. Radiat. Isot.* **2020**, *160*, 109112. [CrossRef]
55. Terray, L.; Gauthier, P.J.; Breton, V.; Giammanco, S.; Sigmarsson, O.; Salerno, G.; Caltabiano, T.; Falvard, A. Radon activity in volcanic gases of Mt. Etna by passive dosimetry. *J. Geophys. Res.* **2020**, *125*, e2019JB019149. [CrossRef]
56. Stojanovska, Z.; Boev, B.; Zunic, Z.S.; Ivanova, K.; Ristova, M.; Tsenova, M.; Ajka, S.; Janevik, E.; Taleski, V.; Bossew, P. Variation of indoor radon concentration and ambient dose equivalent rate in different outdoor and indoor environments. *Radiat. Environ. Biophys.* **2016**, *55*, 171–183. [CrossRef]

57. Elío, J.; Cinelli, G.; Bossew, P.; Gutiérrez-Villanueva, J.L.; Tollefsen, T.; De Cort, M.; Nogarotto, A.; Braga, R. First steps towards an All-European Indoor Radon Map. *Nat. Hazards Earth Syst. Sci.* **2019**, *19*, 2451–2464. [[CrossRef](#)]
58. Giustini, F.; Ciotoli, G.; Rinaldini, A.; Ruggiero, L.; Voltaggio, M. Mapping the geogenic radon potential and radon risk by using Empirical Bayesian Kriging regression: A case study from a volcanic area of central Italy. *Sci. Total Environ.* **2019**, *661*, 449–464. [[CrossRef](#)]
59. Moharram, B. The influence of mechanical vibrations of railway and car traffics on the radon exhalation using track detector technique. In Proceedings of the Seventh Conference of Nuclear Sciences & Applications, Cairo, Egypt, 6–10 February 2000. [[CrossRef](#)]
60. Vaizoglu, S.A.; Güler, Ç. Indoor radon concentrations in Ankara dwellings. *Indoor Built Environ.* **1999**, *8*, 327–331. [[CrossRef](#)]
61. AccuWeather. Available online: <https://www.accuweather.com/es/pe/lima/264120/current-weather/264120> (accessed on 7 May 2023).
62. SENAMHI. Monitoreo de la Calidad de Aire, Para Lima Metropolitana. Available online: <https://www.senamhi.gob.pe/?p=calidad-del-aire> (accessed on 7 May 2023).
63. ALGADE. DPR. Available online: <https://algade.com/en/product/dpr-2/> (accessed on 7 May 2023).
64. Kropat, G.; Bochud, F.; Jaboyedoff, M.; Laedermann, J.P.; Murith, C.; Palacios, M.; Baechler, S. Improved predictive mapping of indoor radon concentrations using ensemble regression trees based on automatic clustering of geological units. *J. Environ. Radioact.* **2015**, *147*, 51–62. [[CrossRef](#)]
65. Ruano-Ravina, A.; Quindós-Poncela, L.; Sainz Fernández, C.; Barros-Dios, J.M. Radón interior y salud pública en España: Tiempo para la acción. *Gac. Sanit.* **2014**, *28*, 439–441. [[CrossRef](#)]
66. Kropat, G.; Bochud, F.; Jaboyedoff, M.; Laedermann, J.P.; Murith, C.; Palacios, M.; Baechler, S. Major influencing factors of indoor radon concentrations in Switzerland. *J. Environ. Radioact.* **2014**, *129*, 7–22. [[CrossRef](#)]
67. Kropat, G.; Bochud, F.; Jaboyedoff, M.; Laedermann, J.P.; Murith, C.; Palacios, M.; Baechler, S. Predictive analysis and mapping of indoor radon concentrations in a complex environment using kernel estimation: An application to Switzerland. *Sci. Total Environ.* **2015**, *505*, 137–148. [[CrossRef](#)] [[PubMed](#)]

Disclaimer/Publisher’s Note: The statements, opinions and data contained in all publications are solely those of the individual author(s) and contributor(s) and not of MDPI and/or the editor(s). MDPI and/or the editor(s) disclaim responsibility for any injury to people or property resulting from any ideas, methods, instructions or products referred to in the content.